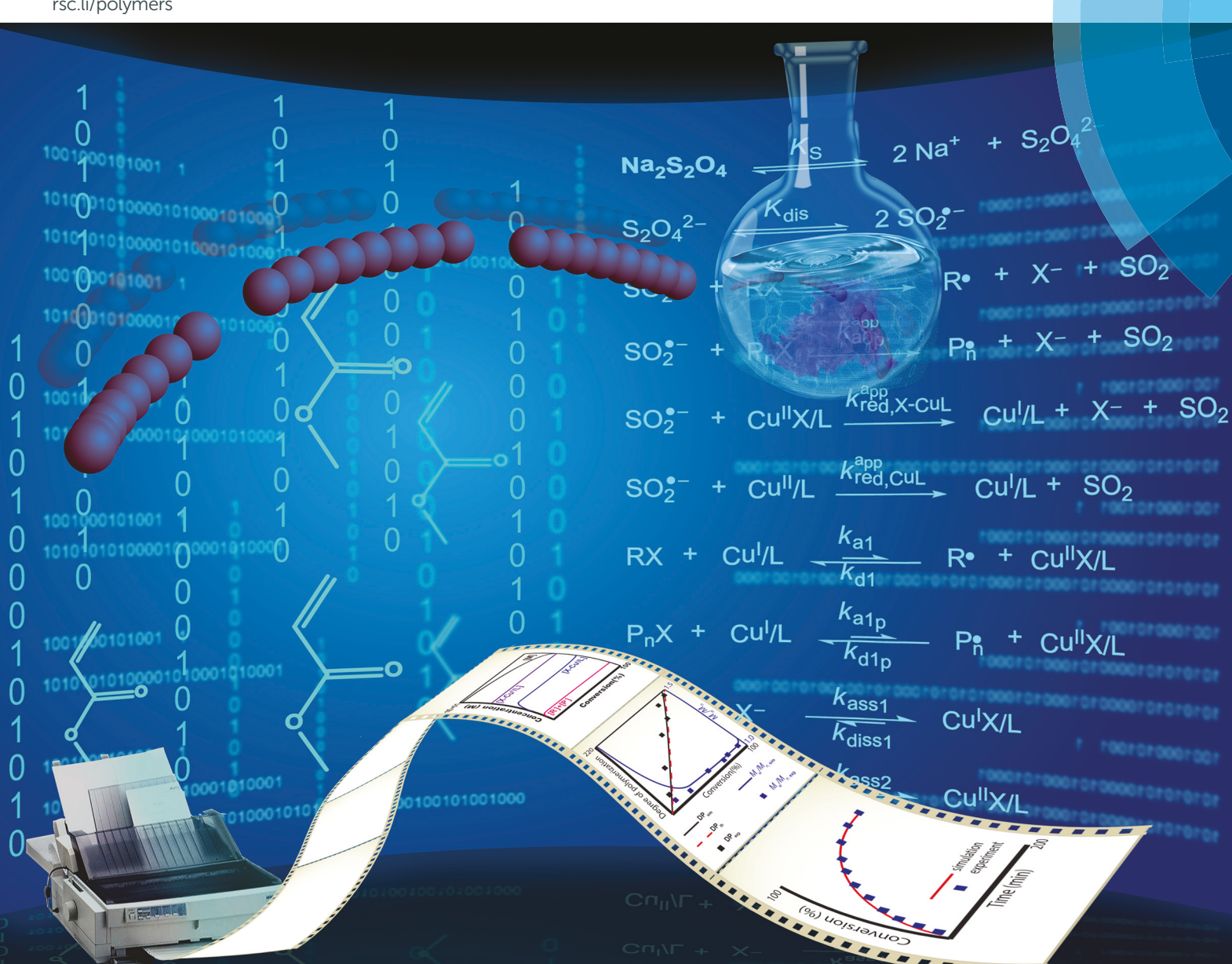
Polymer Chemistry

rsc.li/polymers



ISSN 1759-9962



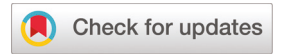
PAPER

Krzysztof Matyjaszewski, Jorge F. J. Coelho et al. Mechanism of supplemental activator and reducing agent atom transfer radical polymerization mediated by inorganic sulfites: experimental measurements and kinetic simulations

Polymer Chemistry



PAPER



Cite this: *Polym. Chem.*, 2017, **8**, 6506

Mechanism of supplemental activator and reducing agent atom transfer radical polymerization mediated by inorganic sulfites: experimental measurements and kinetic simulations†

Pawel Krys,^a Marco Fantin,^a Patrícia V. Mendonça,^b Carlos M. R. Abreu, Da,^b Tamaz Guliashvili,^b Jaquelino Rosa,^b Lino O. Santos,^c Arménio C. Serra, Db Krzysztof Matyjaszewski*^a and Jorge F. J. Coelho D**a,^b

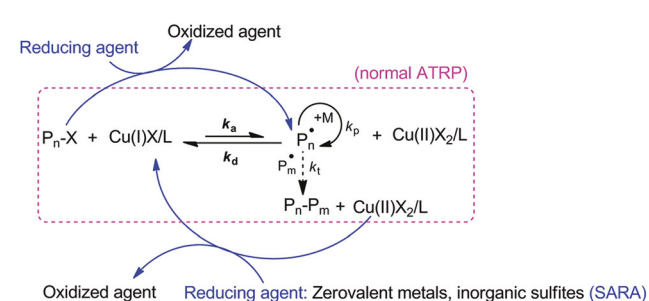
The mechanism of atom transfer radical polymerization (ATRP) mediated by sodium dithionite ($Na_2S_2O_4$), with $Cu^{II}Br_2/Me_6TREN$ as catalyst (Me_6TREN : tris[2-(dimethylamino)ethyl]amine) in ethanol/water mixtures, was investigated experimentally and by kinetic simulations. A kinetic model was proposed and the rate coefficients of the relevant reactions were measured. The kinetic model was validated by the agreement between experimental and simulated results. The results indicated that the polymerization followed the SARA ATRP mechanism, with a SO_2^{+-} radical anion derived from $Na_2S_2O_4$, acting as both supplemental activator (SA) of alkyl halides and reducing agent (RA) for Cu^{II}/L to regenerate the main activator Cu^{II}/L . This is similar to the reversible-deactivation radical polymerization (RDRP) procedure conducted in the presence of Cu^{II}/L . The electron transfer from SO_2^{+-} , to either $Cu^{II}Br_2/Me_6TREN$ or R-Br initiator, appears to follow an outer sphere electron transfer (OSET) process. The developed kinetic model was used to study the influence of targeted degree of polymerization, concentration of $Cu^{II}Br_2/Me_6TREN$ and solubility of $Na_2S_2O_4$ on the level of polymerization control. The presence of small amounts of water in the polymerization mixtures slightly increased the reactivity of the Cu^{II}/L complex, but markedly increased the reactivity of sulfites.

Received 4th August 2017, Accepted 22nd September 2017 DOI: 10.1039/c7py01319a

rsc.li/polymers

Introduction

The field of macromolecular engineering continues to benefit from the progress of reversible deactivation radical polymerization (RDRP) procedures, which provide access to many well-defined polymers. One of the most extensively investigated RDRP techniques is the versatile and robust atom transfer radical polymerization (ATRP) process. In ATRP (Scheme 1), a metal/ligand catalytic complex in a lower oxidation state (typically Cu^I/L) activates a dormant alkyl halide initiator, R–X, or



Scheme 1 General mechanism of Cu^I/L-catalyzed normal ATRP (black arrows) and SARA ATRP (L: ligand and X: halide) (both blue and black arrows).

dormant polymer chain, P_n –X, (where X is a (pseudo)halogen) to form a propagating radical (P_n^{\star}) and the catalytic complex in a higher oxidation state (X–Cu^{II}/L).^{3,6} Then, a few monomer units can add to the growing radical before it is quickly deactivated back to the dormant state by the X–Cu^{II}/L complex.

The original ATRP technique used *ca.* 10 000 ppm of copper in the reaction medium, ⁶ which contaminated the polymer

^aDepartment of Chemistry, Carnegie Mellon University, 4400 Fifth Avenue, Pittsburgh, Pennsylvania 15213, USA. E-mail: jcoelho@eq.uc.pt, km3b@andrew.cmu.edu

^bCEMMPRE, Department of Chemical Engineering, University of Coimbra, 3030-790 Coimbra, Portugal

^cCIEPQPF, Department of Chemical Engineering, Faculty of Sciences and Technology, University of Coimbra, Portugal

[†] Electronic supplementary information (ESI) available: Additional experiments and kinetic simulations, NMR spectra, SEC traces, CV traces and detailed experimental procedures. See DOI: 10.1039/c7py01319a

product and required extensive purification. Several recently developed ATRP procedures use only a few ppm of copper complexes, while maintaining stringent control over the polymerization. These procedures include activators regenerated by electron transfer (ARGET) ATRP, initiators for continuous activator regeneration (ICAR) ATRP, electrochemically mediated ATRP (eATRP), photochemically mediated (photoATRP)¹⁰ and supplemental activator and reducing agent (SARA) ATRP. 11-16 Recently, some metal-free ATRP systems have also been reported. 17-19

SARA ATRP typically employs zerovalent metals (*e.g.*, Cu⁰) that can be easily removed from the reaction media after polymerization. ^{11,12,20,21} During the polymerization, SARA agents act as supplemental activators (SA), directly reacting with the alkyl halides and as reducing agents (RA) continuously regenerating the Cu^I/L activator (Scheme 1). In order to optimize the reaction conditions and scale up the process, it is necessary to understand the polymerization mechanism. Detailed mechanistic studies revealed that the RDRP in the presence of Cu⁰ indeed follows the SARA ATRP mechanism: alkyl halides are predominately activated by the Cu^I/L species, whereas activation by Cu⁰ is supplemental, and Cu^I/L disproportionation is minimal. ^{15,21–24}

More recently, inorganic sulfites, approved by the Food and Drug Administration, ²⁵ were employed as SARA agents to prepare a variety of well-defined (co)polymers. ^{14,26–33} This avoided the continuous generation of soluble Cu species introduced into the system by activation of alkyl halides by Cu⁰ and by comproportionation, effectively retaining a reduced concentration of metal catalyst. ¹⁴ Control experiments revealed that Na₂S₂O₄ can indeed activate alkyl halides as well as reduce Cu^{II}Br₂/L deactivator complex, thus acting as a typical SARA agent, similar to Cu⁰. ^{14,33} However, no detailed mechanistic investigations have been conducted to evaluate the relative contribution of the participating reactions during a SARA ATRP with inorganic sulfites.

The aim of this study was an in-depth investigation of the mechanism of $\rm Na_2S_2O_4$ -mediated SARA ATRP, employing experimental data supplemented by kinetic simulations using PREDICI. The Rate coefficients of the elementary reactions involved in the procedure were quantified. The kinetic simulations revealed an excellent agreement between the simulated and experimental data, supporting the validity of the proposed SARA ATRP mechanism.

Experimental

Materials

 ${\rm Cu^{II}Br_2}$ (Acros, 99+% extra pure, anhydrous), ${\rm Cu^{II}}$ trifluoromethanesulfonate (${\rm Cu^{II}(OTf)_2}$, Sigma-Aldrich, 99%), deuterated chloroform (${\rm CDCl_3}$) (Euriso-top, +1% TMS), diphenyl ether (DPE, Sigma-Aldrich, 99%), ethyl α -bromoisobutyrate (EBiB, Sigma-Aldrich, 98%), ethanol (EtOH, Panreac, 99.5%), methyl 2-bromopropionate (MBrP, Sigma Aldrich, 98%), polystyrene (PS) standards (Polymer Laboratories), and sodium dithionite (Na₂S₂O₄, Aldrich, 85% technical grade) were used

as received. Cu^IBr (Sigma Aldrich, 98%) was washed with glacial acetic acid, followed by 1% HCl solution to remove traces of $Cu^{II}Br_2$. The Cu^IBr was then washed with acetone and dried under a stream of nitrogen before use. Methyl acrylate (MA, Acros, 99% stabilized) was passed through a sand/alumina column before use in order to remove the radical inhibitor. Purified water (Milli-Q®, Millipore, resistivity >18 $M\Omega$ cm, pH_{25} $_{^{\circ}C}$ = 5.6) was obtained by reverse osmosis. THF (Panreac, HPLC grade) was filtered under reduced pressure before use. Tris[2-(dimethylamino)ethyl]amine (Me $_6$ TREN) was synthesized according the procedures described in the literature.³⁷

Methods

Stopped-flow experiments were conducted on a thermostated stopped-flow Hi-Tech model SF-61, Hi-Tech Scientific (Salisbury, UK), equipped with a 50 W Quartz tungsten halogen lamp (Thorn type M32) and a photomultiplier PSP-60 (0–1500 Vdc at 2.5 mA), and a SF-61 single mixing stopped-flow module with two 1 mL Kloehn syringes. Data acquisition and preliminary analysis was accomplished with the IS-2 v.2.3b6 software supplied by Hi-Tech. All measurements were carried out at 30 °C in a cuvette with an optical path length of 1.5 mm. For every measurement, a total volume of 0.15 mL was ejected through the cuvette with a flow-rate of 10 mL s $^{-1}$ (4.4 mm ms $^{-1}$) with a dead-time of 2 ms.

The chromatographic parameters of poly(methyl acrylate) (PMA) were determined using a Viscotek (Viscotek TDAmax) size exclusion chromatography (SEC) equipped with an on-line degasser, a differential viscometer (DV), right-angle laser-light scattering (RALLS, Viscotek), low-angle laser-light scattering (LALLS, Viscotek), and refractive index (RI) detectors. The column set up consisted of a PL-guard column ($50 \times 7.5 \text{ mm}^2$) followed by a Viscotek Tguard (8 µm), Viscotek T2000 (6 µm), Viscotek T3000 (6 μm), and Viscotek LT4000L (7 μm) columns. A dual piston pump was programed with a flow rate of 1 mL min⁻¹. The THF eluent was filtered through a 0.2 μ m filter. The tests were carried out at 30 °C using an Elder CH-150 heater. The samples were filtered through a 0.2 µm polytetrafluoroethylene (PTFE) membrane before the injection (100 µL). Narrow molecular weight (MW) PS standards were used for calibration. The dn/dc value was determined as 0.063 mL g^{-1} for PMA. Molecular weight (M_n^{SEC}) and dispersity $(D = M_w/M_n)$ of the synthesized polymers were determined by multidetector calibration using the OmniSEC software version 4.6.1.354.

¹H NMR spectra were recorded on a Bruker Avance III 400 MHz spectrometer, with a 5 mm TIX triple resonance detection probe, in CDCl₃ with tetramethylsilane (TMS) as an internal standard. MestRenova (v.6.0.2-5475) was employed for the integration of the signals.

Atomic absorption spectroscopy (AAS) was conducted on a PerkinElmer (Model 3300, USA) to evaluate the content of residual copper catalyst in the purified polymers.

A Jasco V-530 spectrophotometer was used for the ultraviolet-visible (UV-Vis) studies and the analysis was carried in the 200–1100 nm range at room temperature. The reaction

mixtures were centrifuged prior to the measurements in order to settle down the Na₂S₂O₄ particles.

Gas chromatography (GC) measurements were conducted using a Shimadzu GC-17A equipped with a FID detector.

Cyclic voltammetry (CV) analyses were conducted in MA/ solvent 2:1 mixtures. The solvents were different EtOH/H2O mixtures (see below). 0.1 M n-Bu₄NPF₆ was added as supporting electrolyte (Alfa Aesar, 99%). CV traces were recorded on a Gamry Reference 600 potentiostat using a three electrode cell with a glassy carbon disk working electrode (diameter = 3 mm), which was polished with a 0.25 µm diamond paste and rinsed in an ultrasound bath for 5 minutes prior to each analysis. The counter electrode was a Pt wire, and the reference electrode was a Saturated Calomel Electrode (SCE). The working solutions were deoxygenated with a N2 purge for at least 15 min prior to analysis, and then kept under a positive N₂ pressure. To prepare the binary Cu^{II}/Me₆TREN complex, the Cu^{II}(OTf)₂ salt was used since OTf⁻ is a weakly coordinating anion. Conversely, Cu^{II}Br₂ was used to prepare the ternary Br-Cu^{II}/Me₆TREN complex. CV simulation was performed with the software Digisim 3.03 (Bioanalytical Systems).

Results and discussion

Kinetic model

The polymerization was studied under the following model experimental conditions: MA as monomer; CuIIBr2/Me6TREN as deactivator complex; Na₂S₂O₄ as SARA agent; EBiB or MBrP as initiators; T = 30 °C and MA/EtOH/H₂O = 2/0.9/0.1 (v/v/v).²⁶ Scheme 2 presents the kinetic model describing the SARA ATRP in the presence of Na₂S₂O₄. The relevant reactions included in the model are based on previously reported experimental and simulation results. 14,21,26-28,33,38,39 Reactions include: dissolution and dissociation of the inorganic sulfite (1, 2); supplemental activation of (macro)alkyl halides by SO₂. (3, 4); reduction of X-Cu^{II}/L and Cu^{II}/L complexes by SO₂. (5, 6), ATRP equilibrium between (macro)alkyl halides and (macro)radicals (7, 8); halidophilicity equilibrium of Cu^I/L and Cu^{II}/L complexes (9, 10); addition of alkyl halide-derived radicals (R') to the monomer (11); propagation (12); termination of two R' radicals (13); termination of R' with a polymer radical (P_n) (14) and termination of two P_n radicals (15). Reaction rate coefficients were either quantified by isolating the respective reactions (vide infra) or based on results provided in previous literature reports.

Model experiments and determination of rate coefficients

The concentration of the SO_2 radical anions resulting from the dissolution of the dithionite salt in the reaction mixture (Scheme 2, reaction (1)) and subsequent dissociation of the dithionite anion (Scheme 2, reaction (2)) strongly depend on the polarity of the reaction mixture. While the exact SO_2 concentration in the polymerization mixture was unknown, this information was not strictly necessary for an accurate kinetic analysis of the system. In fact, rate coefficients of all

1.
$$Na_{2}S_{2}O_{4} \xrightarrow{K_{S}} 2Na^{+} + S_{2}O_{4}^{2-}$$
2. $S_{2}O_{4}^{2-} \xrightarrow{K_{dis}} 2SO_{2}^{\bullet-}$
3. $SO_{2}^{\bullet-} + RX \xrightarrow{k_{a0}^{app}} R^{\bullet} + X^{-} + SO_{2}$
4. $SO_{2}^{\bullet-} + P_{n}X \xrightarrow{k_{a0}^{app}} P_{n}^{\bullet} + X^{-} + SO_{2}$
5. $SO_{2}^{\bullet-} + Cu^{||}X/L \xrightarrow{k_{app}^{app}} Cu^{||}L + X^{-} + SO_{2}$
6. $SO_{2}^{\bullet-} + Cu^{||}/L \xrightarrow{k_{a1}^{app}} R^{\bullet} + Cu^{||}X/L$
7. $RX + Cu^{||}/L \xrightarrow{k_{a1}^{app}} R^{\bullet} + Cu^{||}X/L$
8. $P_{n}X + Cu^{||}/L \xrightarrow{k_{a1}^{app}} P_{n}^{\bullet} + Cu^{||}X/L$
9. $Cu^{||}/L + X^{-} \xrightarrow{k_{ass1}^{app}} Cu^{||}X/L$
10. $Cu^{||}/L + X^{-} \xrightarrow{k_{ass2}^{app}} Cu^{||}X/L$
11. $R^{\bullet} + M \xrightarrow{k_{add}^{app}} P_{1}^{\bullet}$
12. $P_{n}^{\bullet} + M \xrightarrow{k_{p}^{app}} P_{n+1}^{\bullet}$
13. $R^{\bullet} + R^{\bullet} \xrightarrow{k_{t0}^{app}} R^{-}R^{-}R$
14. $R^{\bullet} + P_{n}^{\bullet} \xrightarrow{k_{t}^{app}} D_{(n+m)}$

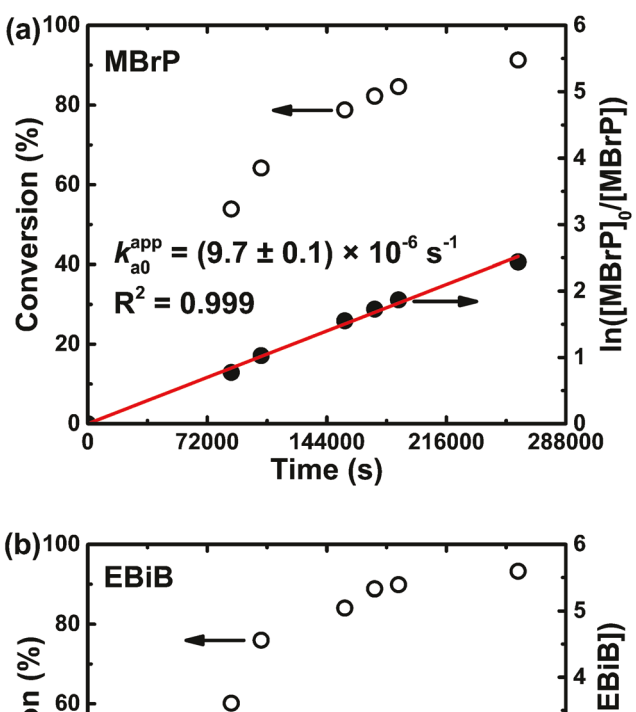
Scheme 2 Kinetic model for the SARA ATRP mediated by $Na_2S_2O_4/Cu^{II}Br_2/L$ (L = Me_6TREN).

reactions involving SO_2 were measured as apparent rate coefficients $k^{app} = k \times [SO_2$], considering constant $[SO_2$] during polymerization. This is a reasonable assumption, because the solubility of $Na_2S_2O_4$ in the polymerization mixtures is very low and, therefore, the presence of some undissolved salt can supply a continuous amount of $S_2O_4^{2-}$ and SO_2 to the system. This was confirmed by experiments: the semilogarithmic kinetic plots for the reaction between $Na_2S_2O_4$ and RX were linear, indicating the presence of a constant concentration of reducing agent, SO_2 (Fig. 1).

The SO₂. radical anion can be involved in three main reactions, described in the next three sections: (i) addition to monomer, resulting in initiation of new polymer chains; (ii) supplemental activation of initiator (Scheme 2, reaction (3)) or dormant chain-end (Scheme 2, reaction (4)), and (iii) continuous reduction of the Cu^{II}/L complexes (Scheme 2, reactions (5) and (6)). These reactions were investigated in model experiments.

Contribution of SO₂'- to the direct initiation of growing chains

Previous studies showed that MA can be polymerized in dimethyl sulfoxide (DMSO) at 30 °C in the presence of $Na_2S_2O_4$, which served as source of SO_2 . However, the reaction was slow, reaching only $\approx 8\%$ maximum monomer convertion.



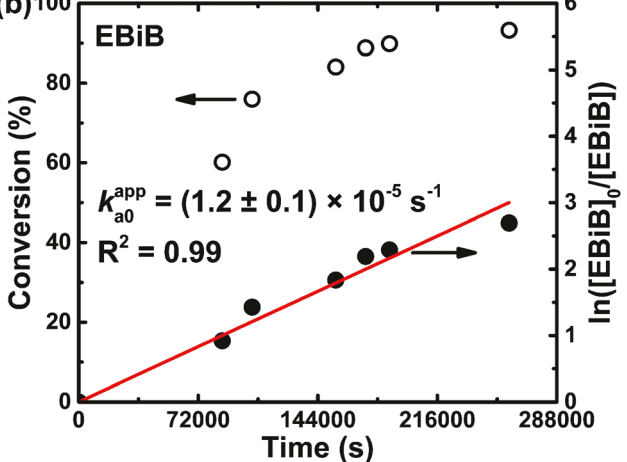


Fig. 1 Kinetic plots of conversion and $ln[RBr]_0/[RBr]$ vs. time for the activation of (a) MBrP or (b) EBiB by the radical anion SO_2 . (derived from the dissociation of $Na_2S_2O_4$). Conditions: MeOAc/EtOH/ $H_2O=2/0.9/0.1$ (v/v/v) at 30 °C; [MeOAc] $_0/[MBrP$ or EBiB] $_0/[Na_2S_2O_4]_0=222/1/1$.

sion after 8 h, and the resulting polymer had a high molecular weight and a very broad molecular weight distribution (MWD, $M_{\rm w}/M_{\rm n}=4.55$). The slow polymerization rate suggested that, under SARA ATRP conditions, the rate of initiation of new polymer chains by SO₂. was negligible. In an EtOH/H₂O mixture the reaction was much slower, with only 2% monomer conversion after 8 days. Fig. S1† shows that the apparent rate coefficient of propagation ($k_{\rm p}^{\rm app}=k_{\rm p}[{\rm R}^{\star}]$) under conditions MA/EtOH/H₂O = 2/0.9/0.1 (v/v/v) at 30 °C initiated only by SO₂. was (2.9 ± 0.1) × 10⁻⁸ s⁻¹. This clearly indicates that the contribution of Na₂S₂O₄ to the direct initiation of growing chains during SARA ATRP was insignificant in comparison with other reactions involved in the polymerization procedure.

Determination of rate coefficients of activation of (macro)alkyl halides by SO_2 (k_{a0}^{app}) and $k_{a0p}^{app})$

In "normal" ATRP systems, the alkyl halide initiator and the dormant polymeric species are exclusively activated by the Cu^I/L

complex. 21,22,24 In SARA ATRP, however, they can also be activated by the SARA agent. This supplemental activation was confirmed using a model system, in the absence of Cu species, for the polymerization of MA in the presence of the initiator (EBiB) and Na₂S₂O₄ in MA/EtOH/H₂O = 2/0.9/0.1 (v/v/v) at 30 °C (Fig. S2†). As expected, the polymerization was not controlled, forming a polymer with broad MWD ($M_{\rm w}/M_{\rm n} > 2$), because no X–Cu^{II}/L deactivator species was present in the reaction. The ¹H NMR spectrum of the prepared PMA (Fig. S3†) confirmed the presence of initiator fragments in the polymer chains validating that the polymerization was initiated by the EBiB-derived radicals, resulting from the activation of EBiB by SO₂. –

The activation rate coefficients of alkyl halides by SO_2 ($k_{a0}^{\rm app}$, Scheme 2, reaction (3)) for EBiB and MBrP (in the absence of Cu species) were determined using model systems, where MA was replaced by methyl acetate (MeOAc) to mimic the reaction medium while avoiding any possible polymerization. The reaction was irreversible because of the fast termination reactions between the generated tertiary isobutyryl or secondary propionyl radicals. To obtain $k_{a0}^{\rm app}$, the rate of consumption of the initiator, EBiB or MBrP, was measured by GC (Fig. 1). The value of $k_{a0}^{\rm app}$ (the slope of the plot of $\ln[{\rm RBr}]_0/[{\rm RBr}] \nu s$. time) was calculated to be $(9.7 \pm 0.1) \times 10^{-6} {\rm s}^{-1}$ and $(1.2 \pm 0.1) \times 10^{-5} {\rm s}^{-1}$ for MBrP and EBiB, respectively.

It was envisioned that SO2 - could also activate dormant polymer chains during the polymerization. To test this hypothesis, a PMA-Br macroinitiator was synthesized using a typical Na₂S₂O₄/Cu^{II}Br₂/Me₆TREN-catalyzed SARA ATRP reaction. ^{14,26} A copper-free PMA-Br macroinitiator was obtained (% copper = 0.02 ppm determined by AAS; $M_n^{SEC} = 6.6 \times 10^3$; $M_n^{th} = 6.7 \times 10^3$; $M_{\rm p}^{\rm NMR} = 7.0 \times 10^3$; chain-end functionality = 99%) after extensive purification by dialysis. Subsequently, chain extension of the macroinitiator using only Na2S2O4 as the activator (in the absence of the Cu^{II}Br₂/Me₆TREN complex) was examined. The shift of the SEC trace towards higher molecular weight value (Fig. S4†) confirmed that SO₂ acted as a supplemental activator of the dormant PMA-Br chains. It is worth mentioning that no copper source was available in this experiment, so that SO₂. was the only possible activator. For kinetic modeling, the value of activation rate coefficient of PMA-Br chains by $SO_2^{\bullet-}$ (k_{a0n}^{app} , Scheme 2, reaction (4)) was assumed to be identical to the value obtained for the MBrP initiator $(k_{a0}^{app} = (9.7 \pm 0.1) \times 10^{-6} \text{ s}^{-1}),$ since the two species have similar structures.

Determination of the rate coefficient reduction of $\mathrm{Cu^{II}/L}$ by $\mathrm{SO_2^{--}}(k_\mathrm{red}^\mathrm{app})$

In a typical SARA ATRP process, the Cu^{II}/L complex is slowly reduced *in situ* by the SARA agent to regenerate the Cu^I/L activator (Scheme 2, reactions (5) and (6)). In this work, the rates of reduction of Cu^{II}Br₂/Me₆TREN and Cu^{II}(OTf)₂/Me₆TREN by the SO₂· radical anion were measured in a MeOAc/EtOH/H₂O mixture, thereby mimicking the polymerization conditions. UV-Vis spectroscopy showed a continuous decrease of the Cu^{II}Br₂/Me₆TREN and Cu^{II}(OTf)₂/Me₆TREN absorbance band over time, confirming the reducing properties of SO₂· (Fig. 2a

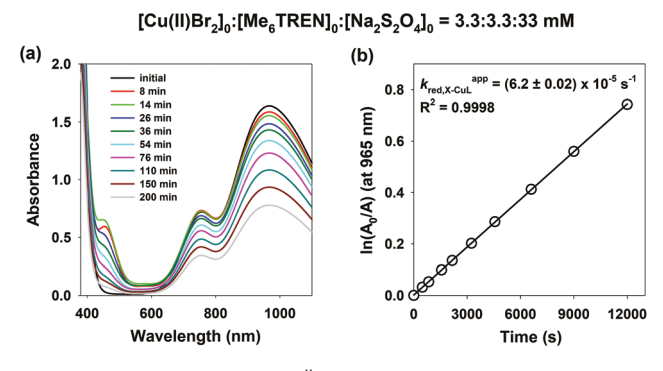


Fig. 2 (a) UV-Vis spectra of $Cu^{II}Br_2/Me_6TREN$ during the reduction by $Na_2S_2O_4$ in a MeOAc/EtOH/ $H_2O=2/0.9/0.1$ (v/v/v) mixture at 30 °C and (b) determination of the $k_{\rm red,X-CuL}^{\rm app}$. Conditions: $[Cu^{II}Br_2]_0/[Me_6TREN]_0/[Na_2S_2O_4]_0=0.1/0.1/1$; $[Cu^{II}Br_2]_0=3.3$ mM.

and Fig. S5a†). A similar behaviour was previously observed using DMSO as solvent. The reduction rate coefficients $k_{\rm red,X-CuL}^{\rm app} = (6.2 \pm 0.02) \times 10^{-5} \ {\rm s}^{-1}$ and $k_{\rm red,CuL}^{\rm app} = (2.3 \pm 0.02) \times 10^{-4} \ {\rm s}^{-1}$ for Cu^{II}Br₂/Me₆TREN and Cu^{II}(OTf)₂/Me₆TREN, respectively, were determined from the rate of the decrease of absorption (Fig. 2b and Fig. S5b†).

Determination of halidophilicity equilibrium constants $(K_{Br}^{I} \text{ and } K_{Br}^{II})$

The equilibrium constant of association of Br to CuII/ Me₆TREN ($K_{Br}^{II} = k_{ass2}/k_{diss2}$, also termed the halidophilicity constant, Scheme 2, reaction (10)), was determined by spectrophotometric titration of the copper complex with n-Bu₄NBr (Fig. S6†). A value of $K_{\rm Br}^{\rm II} = (1.65 \pm 0.19) \times 10^4 \, {\rm M}^{-1}$ was determined in MA/EtOH/ $H_2O = 2/0.9/0.1$ (v/v/v). The obtained $K_{\rm Br}^{\rm HI}$ value, measured in the presence of a small amount of water (3.3% of the total volume), was in between the values measured for $K_{\rm Br}^{\rm II}$ in pure organic solvent (1.26 × 10⁶ M⁻¹ in MeCN)⁴¹ and in pure water (4.26 M⁻¹).⁴² Despite the decrease in K_{Br}^{II} with respect to the value in MeCN, the Br-Cu^{II}/ Me₆TREN deactivator complex was still very stable and did not significantly dissociate in the presence of MA/EtOH/H₂O = 2/0.9/0.1 (v/v/v). Under polymerization conditions, only <2% of Br-Cu^{II}/Me₆TREN dissociated to form Br⁻ + Cu^{II}/Me₆TREN, the latter being an ineffective deactivator.

The $K_{\rm Br}^{\rm I}$ equilibrium constant (Scheme 2, reaction (9)) was determined from CV data by applying the following equation:⁴³

$$E_{\mathrm{Br-Cu(II)L/Br-Cu(I)L}}^{\circ} = E_{\mathrm{Cu(II)L/Cu(I)L}}^{\circ} + \frac{RT}{F} \ln \frac{K_{\mathrm{Br}}^{\mathrm{I}}}{K_{\mathrm{Br}}^{\mathrm{II}}} \tag{1}$$

where R is the gas constant, F is the Faraday constant, and $E_{\text{Cu(II)L/Cu(I)L}}^{\circ}$ and $E_{\text{Br-Cu(II)L/Br-Cu(I)L}}^{\circ}$ are the standard reduction potentials of the $\text{Cu}^{\text{II}}/\text{Me}_{6}\text{TREN}$ and $\text{Br-Cu}^{\text{II}}/\text{Me}_{6}\text{TREN}$ complexes, respectively. Both complexes exhibited a reversible reduction in MA/EtOH/H $_2$ O = 2/0.9/0.1 (v/v/v) (Fig. 3), and their reduction potentials (E°) were calculated from their half-wave potentials: $E^{\circ} \approx E_{1/2} = (E_{\text{pc}} + E_{\text{pa}})/2$, where E_{pc} and E_{pa} are the cathodic and anodic peak potential,

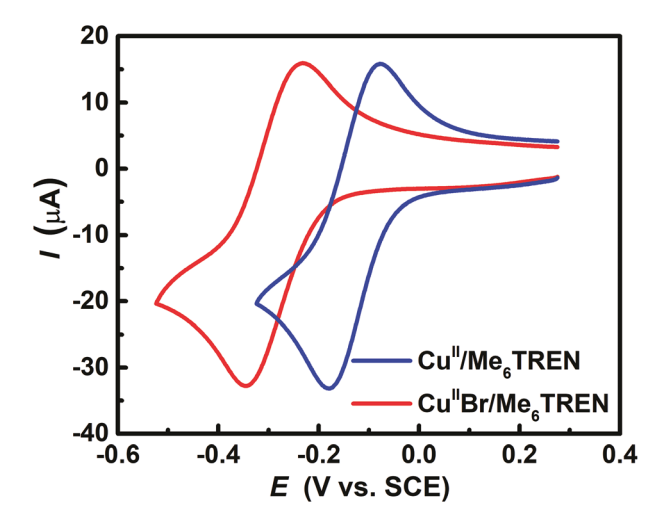


Fig. 3 CV of 2×10^{-3} M Cu^{II}(OTf)₂/Me₆TREN in MA/EtOH/H₂O = 2/0.9/0.1 (v/v/v) + 0.1 M n-Bu₄NPF₆, recorded in the absence and in the presence of 4×10^{-3} M n-Bu₄NBr, at 30 °C and scan rate v = 0.1 V s⁻¹.

respectively (Table 1). A value for $K_{\rm Br}^{\rm I} = 32.6~{\rm M}^{-1}$ was obtained from eqn (1), which is in accordance with previous literature reports in both water and organic solvents, 10 ${\rm M}^{-1} < K_{\rm Br}^{\rm I} < 10^2~{\rm M}^{-1}.$

Determination of rate coefficients of activation of alkyl halides by $\mathrm{Cu^I/L}\ (k_{\mathrm{a}1})$

Due to the fast rate of reaction between RX and Cu^{I}/L it was not possible to directly measure the Cu^{I} activation rate coefficient (k_{a1} , Scheme 2, reaction (7)) by stopped-flow technique. However, k_{a1} values could be determined by CV *via* the homo-

Table 1 Rate coefficients for the modeling of $Na_2S_2O_4/Cu^{11}Br_2/Me_6TREN$ -catalyzed SARA ATRP of MA at 30 °C in EtOH/H₂O. Conditions: MA/EtOH/H₂O = 2/0.9/0.1 (v/v/v); initiator: MBrP or EBiB

Parameter	MBrP	EBiB
$k_{a0} \times [SO_2^{\bullet-}]$	$9.7 \times 10^{-6} \text{ s}^{-1}$	$1.2 \times 10^{-5} \text{ s}^{-1}$
$k_{\text{a0p}} \times [\text{SO}_2^{\bullet,-}]$	$9.7 \times 10^{-6} \text{ s}^{-1}$	$9.7 \times 10^{-6} \text{ s}^{-1}$
k_{a1}	$6.3 \times 10^3 \mathrm{M}^{-1} \mathrm{s}^{-1}$	$1.3 \times 10^5 \text{ M}^{-1} \text{ s}^{-1}$
k_{a1p}	$6.3 \times 10^3 \mathrm{M}^{-1} \mathrm{s}^{-1}$	$6.3 \times 10^3 \mathrm{M}^{-1} \mathrm{s}^{-1}$
$k_{\rm red,X-CuL} \times [{\rm SO_2}^{\bullet-}]$	6.2×1	0^{-5} s^{-1}
$k_{\rm red,CuL} \times [SO_2^{\bullet-}]$	2.3×1	0^{-4} s^{-1}
$K_{ m ATRP}$	1.7×10^{-4} a	$3.5 \times 10^{-3 \ b}$
k_{d1}	$3.7 \times 10^7 \mathrm{M}^{-1} \mathrm{s}^{-1}$	$3.7 \times 10^7 \text{ M}^{-1} \text{ s}^{-1}$
$k_{\rm d1p}$	$3.7 \times 10^7 \mathrm{M}^{-1} \mathrm{s}^{-1}$	$3.7 \times 10^7 \text{ M}^{-1} \text{ s}^{-1}$
k _p	1.47×10^{4}	$^{4} M^{-1} s^{-1} c$
$k_{\mathrm{add}}^{\mathrm{r}}$	$1.84 \times 10^4 \mathrm{M}^{-1} \mathrm{s}^{-1} d$	$1.38 \times 10^{3} \text{ M}^{-1} \text{ s}^{-1} e$
$k_{\rm t}$	2.45×10^{8}	$^{3} M^{-1} s^{-1} f$
k_{tR}	1×10^8 I	$M^{-1} s^{-1} g$
$k_{\rm to}$	$2 \times 10^9 \text{ M}^{-1} \text{ s}^{-1} \text{ g}$	$8 \times 10^{8} \text{ M}^{-1} \text{ s}^{-1 h}$
k_{ass1}	1×10^9]	$M^{-1} s^{-1 i}$
$k_{ m diss1}$	3.1 × 1	$0^7 s^{-1} i$
$k_{\rm ass2}$	1×10^9 l	$M^{-1} s^{-1 j}$
k _{diss2}	6.1 × 1	$0^4 \text{ s}^{-1 j}$

 a Measured. b $K_{\rm ATRP}=k_{\rm a1}/k_{\rm d1}.$ c Ref. 67. d Ref. 64. e Ref. 63. f Ref. 65. g Ref. 39. h Ref. 66. i $K_{\rm Br}^{\rm l}=32.6$ M $^{-1}.$ j $K_{\rm Br}^{\rm ll}=1.65\times10^4$ M $^{-1}.$ $k_{\rm ass1}$ and $k_{\rm ass2}$ were assumed to be fast, as association/dissociation equilibria typically constitute a pre-equilibrium for the ATRP activation step. 21,55

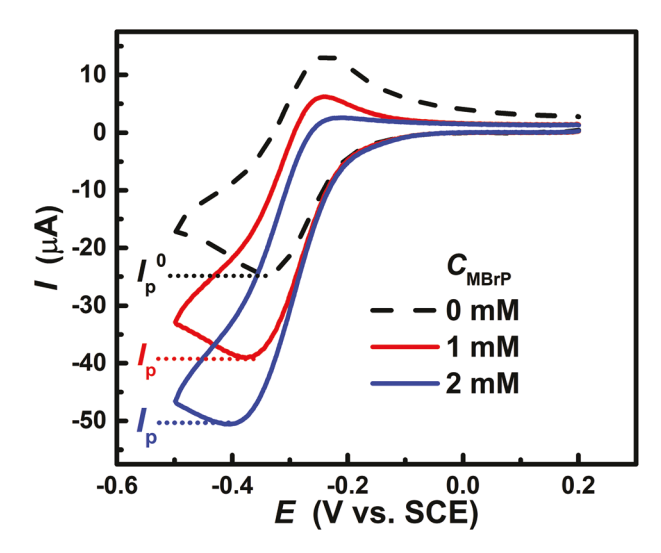
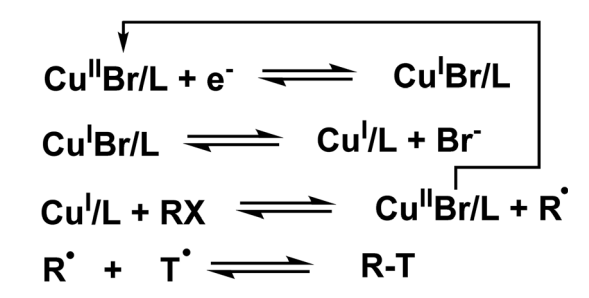


Fig. 4 CV of 1.0×10^{-3} M Cu^{II}Br₂/Me₆TREN in MA/EtOH/H₂O = 2/0.9/0.1 (v/v/v) + 0.1 M n-Bu₄NPF₆ at 30 °C, CV recorded at v = 0.2 V s⁻¹ in the absence and presence of MBrP.

geneous redox catalysis method (Fig. 4). $^{44-46}$ This method has been previously applied to the determination of rate coefficients of fast activation reactions between alkyl halides and various catalysts. $^{47-51}$

As shown in Fig. 4, addition of RX to a solution of $\mathrm{Cu^{II}Br/Me_6TREN}$ completely modified the voltammetric pattern of the complex; the cathodic peak increased in intensity while the anodic peak disappeared. In addition, the cathodic current increased with the concentration of RX (Fig. 4), while it decreased with increasing scan rate (ν , Fig. 87†). This behaviour is typical of an electrochemical processes involving a catalytic cycle in which the electroactive species (the catalyst) is rapidly regenerated near the electrode. The resulting increased cathodic current is related to the activity (k_{a1}) of the catalytic system. The proposed reaction mechanism for the catalytic activation of RX by $\mathrm{Cu^I/L}$ is presented in Scheme 3.

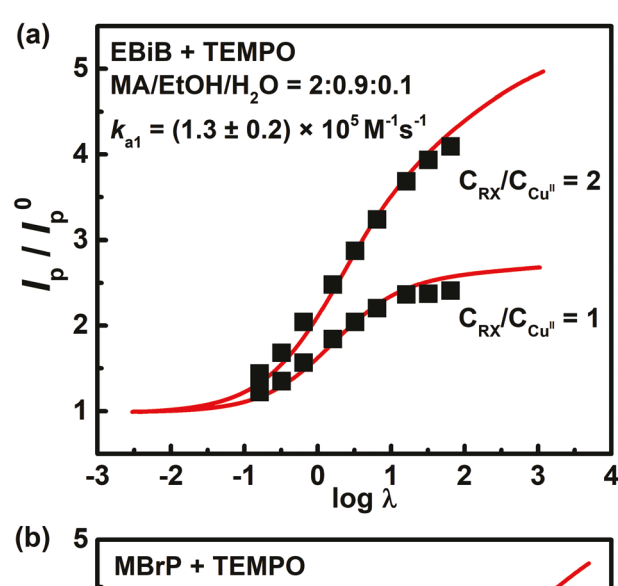
The $k_{\rm a1}$ value can be calculated by examining the catalytic current enhancement defined as $I_{\rm p}/I_{\rm p}^0$, where $I_{\rm p}$ and $I_{\rm p}^0$ stand for the cathodic peak current of the catalyst measured in the presence and absence of RX, respectively (see Fig. 4). $I_{\rm p}/I_{\rm p}^0$ depends on the $k_{\rm a1}$, on the scan rate, and on the ratio between the concentrations of initiator and catalyst $(C_{\rm RX}/C_{\rm Cu}^{\rm II})$. All of



Scheme 3 Catalytic activation of RX by Cu¹/L.

these parameters can be taken into account by considering the dependence of $I_{\rm p}/I_{\rm p}^0$ on a kinetic parameter, $\lambda=RTk_{\rm a1}C_{\rm Cu}^{\rm II}/F\nu$, where R is the gas constant and F is the Faraday constant. Theoretical curves relating $I_{\rm p}/I_{\rm p}^0$ to λ were initially constructed to determine $k_{\rm a1}$. The curves were obtained by digital simulation of CV of a catalytic system following the reaction mechanism in Scheme 3 (see ESI†). Then, the rate coefficient $k_{\rm a1}$ was obtained by comparing the theoretical curves to the experimental $I_{\rm p}/I_{\rm p}^0$ values (Fig. 5). The detailed procedure used to construct the theoretical curves and to fit the experimental $I_{\rm p}/I_{\rm p}^0$ data is described in the ESI.†

Activation rate coefficients $k_{a1} = (1.3 \pm 0.2) \times 10^5 \text{ M}^{-1} \text{ s}^{-1}$ and $(6.3 \pm 0.9) \times 10^3 \text{ M}^{-1} \text{ s}^{-1}$ were determined for the reaction of Cu^I/Me₆TREN with EBiB and MBrP, respectively. These values were 3–10 times higher than k_{a1} in acetonitrile, which stabilizes Cu^I and therefore is generally characterized by lower catalytic activity.⁵⁵ On the other hand, these k_{a1} values were about one order of magnitude lower than k_{a1} in aqueous



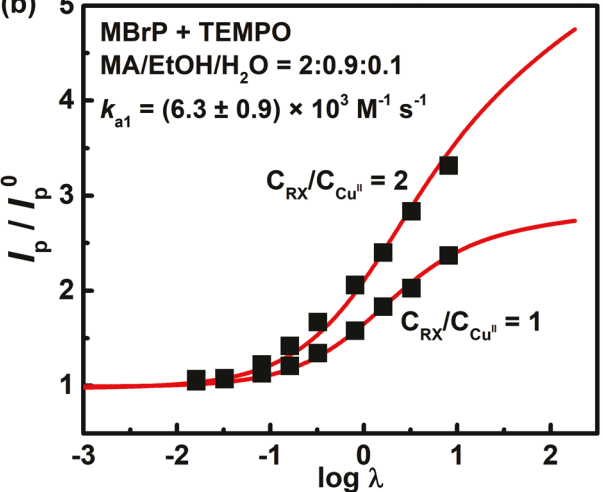


Fig. 5 Determination of $k_{\rm a1}$ for the reaction of Cu^I/Me₆TREN⁺ with (a) EBiB and (b) MBrP in MA/EtOH/H₂O = 2/0.9/0.1 (v/v/v), by fitting of the experimental $I_{\rm p}/I_{\rm p}^0$ (black squares) on theoretical curves (red lines) at 30 °C.

systems, where water is *ca.* 80% of the total volume.²¹ It should be noted that for kinetic modelling the same activation parameter $k_{\rm a1} = k_{\rm a1p} = (6.3 \pm 0.9) \times 10^3 \ {\rm M}^{-1} \ {\rm s}^{-1}$ was used for the activation of the MBrP and PMA–Br chain-end (Scheme 2, reactions (7) and (8), respectively), due to similarity in structure and reactivity.⁵⁶

Interestingly, an approximately twice higher value for $k_{\rm a1}$ was determined when using MeOAc instead of MA, $k_{\rm a1}=(2.9\pm0.4)\times10^5~{\rm M}^{-1}~{\rm s}^{-1}$ and $(1.1\pm0.2)\times10^4~{\rm M}^{-1}~{\rm s}^{-1}$ for EBiB and MBrP, respectively (Fig. S8 and S9†) despite the fact that MeOAc and MA are characterized by nearly identical structures and polarities, $\varepsilon=6.7^{57}$ and $6.8,^{58}$ respectively. Therefore, the significant difference in reactivity is attributable to the presence of the double bond in MA. The monomer stabilizes the Cu^I oxidation state of the catalyst complex by complexation through π -interaction, which lowers the catalyst's reactivity. Indeed, stable complexes between olefins and Cu^I/N,N,N',N'', N''-pentamethyldiethylenetriamine (PMDETA) have been reported. This result also highlights the point that Cu^I complexes must be studied in the presence of monomer to accurately determine their reactivity towards RX activation.

Determination of ATRP equilibrium constant (K_{ATRP}) and rate coefficient of deactivation of radicals by X-Cu^{II}/L (k_{d1})

The ATRP equilibrium constant ($K_{\rm ATRP}$) for the polymerization of MA catalysed by Cu^I/Me₆TREN (with MBrP as initiator) was measured via a modified Fischer's equation using the stopped-flow technique, following the procedures described in the literature (Fig. S10†). A value of $K_{\rm ATRP} = (1.7 \pm 0.05) \times 10^{-4}$ was obtained. Rate coefficient of deactivation of radicals by X–Cu^{II}/L ($k_{\rm d1}$, Scheme 2, reaction (7)) was determined to be (3.7 ± 0.54) × 10⁷ M⁻¹ s⁻¹ for propionyl radicals, using the relation $K_{\rm ATRP} = k_{\rm a1}/k_{\rm d1}$. The same value was used for the deactivation rate coefficient of the PMA radical ($k_{\rm d1p}$, Scheme 2, reaction (8)) due to structure similarity.

It was not possible to determine $K_{\rm ATRP}$ for the reaction between ${\rm Cu^I/Me_6TREN}$ and EBiB by applying the same technique, *i.e.* by fitting to the modified Fischer's equation. This is because during polymerization (*i.e.*, in the presence of MA) EBiB is quickly converted to a PMA–Br chain-end, which has a different structure and reactivity. In this case, an approximation was introduced and $k_{\rm d1}$ was considered to be similar for both MBrP and EBiB, since $k_{\rm d1}$ is roughly constant for radicals derived from different alkyl halides. Therefore, for EBiB the equilibrium constant was estimated as $K_{\rm ATRP} = k_{\rm a1}/k_{\rm d1} = (1.3 \pm 0.2) \times 10^5 \, {\rm M}^{-1} \, {\rm s}^{-1}/(3.7 \pm 0.54) \times 10^7 \, {\rm M}^{-1} \, {\rm s}^{-1} = (3.5 \pm 0.74) \times 10^{-3}$.

The rate coefficients of propagation ($k_{\rm p}$, Scheme 2, reaction (12)), addition of R to monomer ($k_{\rm add}$ Scheme 2, reaction (11)) and radical termination ($k_{\rm to}$, $k_{\rm tR}$, and $k_{\rm t}$, Scheme 2, reactions (13)–(15)) are available in the literature. ^{39,63–67} Although the presence of water can influence the value of $k_{\rm p}$, ⁶⁸ this effect was neglected due to low water content in the studied polymerization systems. Solvent effects on $k_{\rm add}$ could also be neglected since in ATRP initiators are typically quickly consumed at the onset of the reaction. Therefore, the rate of addition of

initiator based radicals to monomers should have limited influence on the bulk of the process. Finally, termination rate coefficients are dependent on the reaction viscosity and chain length.⁶⁹ However, due to the lack of chain-length dependent values, average values were used. Table 1 presents the list of all rate coefficients used in the kinetic model (Scheme 2).

Kinetic model validation

The developed kinetic model was validated by comparing the experimental results of polymerizations, initiated by either EBiB or MBrP, with the results obtained from PREDICI simulations. Experimental and simulated results agreed very well in terms of monomer conversion and evolution of degree of polymerization (DP) and $M_{\rm w}/M_{\rm n}$ with conversion, during a typical Na₂S₂O₄/Cu^{II}Br₂/Me₆TREN-catalyzed SARA ATRP of MA in MA/EtOH/H₂O = 2/0.9/0.1 (v/v/v) at 30 °C initiated by EBiB (Fig. 6). The kinetic model was then further validated under different reaction conditions (see below). These results suggest that the kinetic model in Scheme 2 can provide valid results

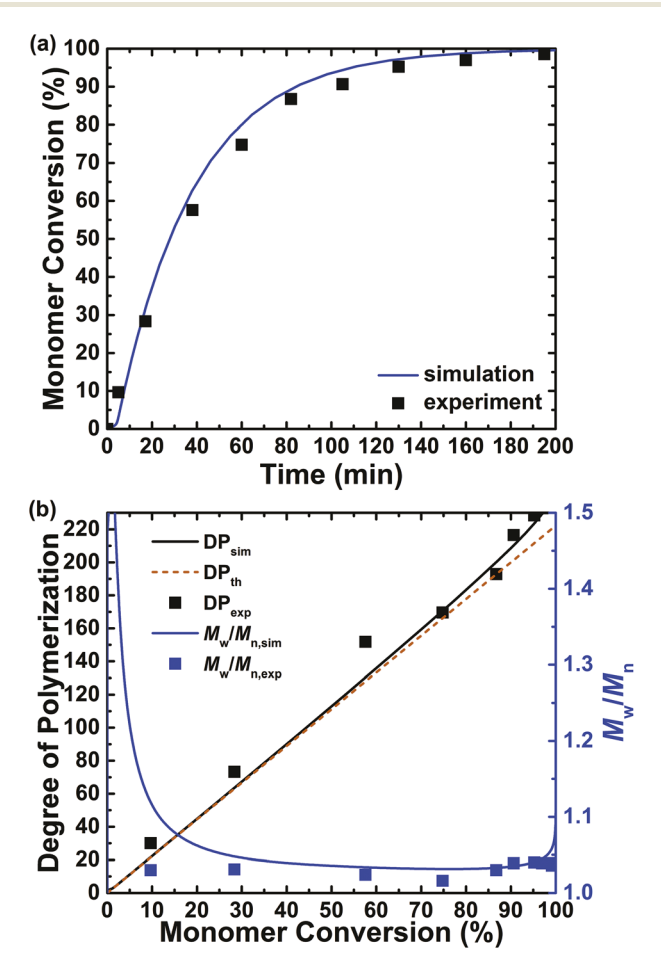


Fig. 6 Comparison of experimental data (symbols) with simulated results (lines) for SARA ATRP of MA in EtOH/H $_2$ O at 30 °C. (a) Monomer conversion vs. time and (b) number-average degree of polymerization (DP $_n$) and $\mathcal D$ vs. monomer conversion. Reaction conditions: MA/EtOH/H $_2$ O = 2/0.9/0.1 (v/v/v); [MA] $_0$ /[EBiB] $_0$ /[Na $_2$ S $_2$ O $_4$] $_0$ /[Cu II Br $_2$] $_0$ /[Me $_6$ TREN] $_0$ = 222/1/1/0.1/0.2, [MA] $_0$ = 7.4 M.

that provide a better understanding of the $Na_2S_2O_4/Cu^{II}Br_2/Me_6TREN$ -catalyzed SARA ATRP mechanism.

An induction period was observed experimentally in the case of a polymerization initiated by MBrP, which was not accounted for in the kinetic model. This behaviour might stem from the impurities in the $\rm Na_2S_2O_4$ (only 85% pure), which could cause partial re-oxidation of the reagents. Indeed, induction periods of various lengths were observed for different batches of $\rm Na_2S_2O_4$ (Fig. S11†). However, after the induction period ended, the simulated monomer conversion matched the experimental data, while simulated MW agreed well with theoretical and experimental values (Fig. S12†). The formation of side products during the induction period might lead to transfer reactions, which could explain slightly higher experimental $M_{\rm w}/M_{\rm n}$ values as compared to the simulated ones. Since activation of EBiB is faster, an induction period was not observed in this case.

Kinetic simulations were also used to determine the contribution of all reactions to the polymerization. Fig. 7 shows con-

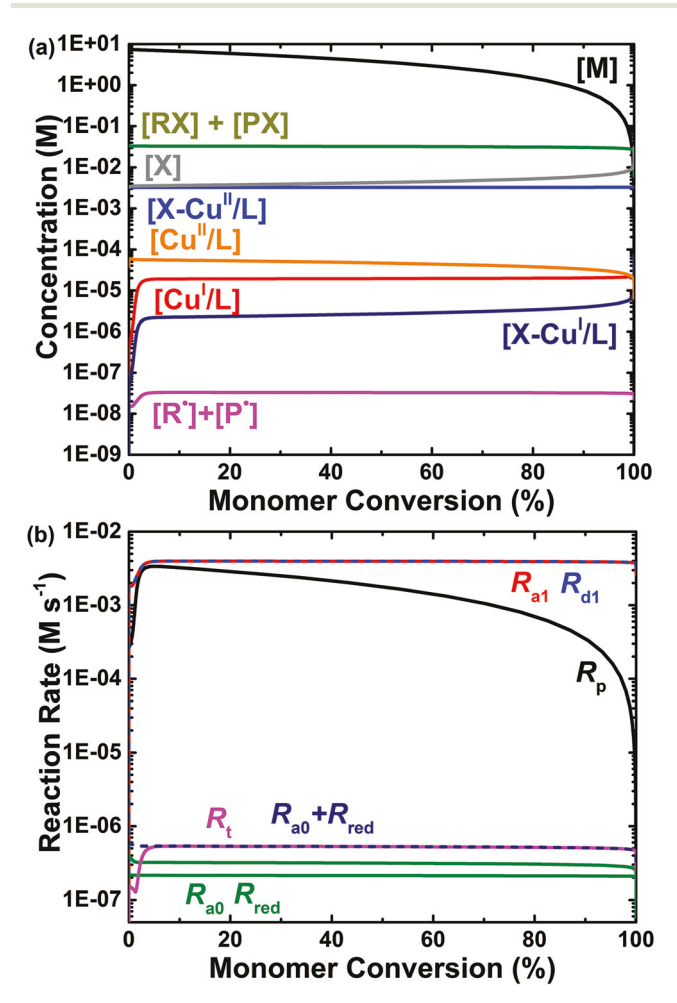


Fig. 7 (a) Simulated concentration of species and (b) calculated reaction rates for the SARA ATRP of MA in EtOH/H₂O at 30 °C. Reaction conditions: MA/EtOH/H₂O = 2/0.9/0.1 (v/v/v); [MA]₀/[EBiB]₀/[Na₂S₂O₄]₀/[Cu^{II}Br₂]₀/[Me₆TREN]₀ = 222/1/1/0.1/0.2, [MA]₀ = 7.4 M.

centrations of reagents and reaction rates determined from simulations of polymerizations initiated by EBiB. The concentration of dormant alkyl halides ([RX] + [PX]) was nearly constant throughout the reaction, indicating high retention of chain-end functionality (Fig. 7a). Furthermore, the concentration of the deactivator complex X-Cu^{II}/L was high enough to efficiently control the polymerization, without the need for additional halide salts. Fig. 7b shows the reaction rates, calculated from relevant rate coefficients and concentrations of the reagents. The dominant reactions were propagation (R_p) , activation of alkyl halides by Cu^{I}/L (R_{a1}), and deactivation of radicals by X-Cu^{II}/L (R_{d1}). Activation and deactivation remained balanced during the entire polymerization, indicating that the ATRP equilibrium was maintained. Activation of alkyl halides by $SO_2^{\bullet-}(R_{a0})$ and reduction of $Cu^{II}(R_{red})$ were supplemental reactions, which occurred ca. 4 orders of magnitude slower than catalyst activation and deactivation. The sum of R_{a0} and $R_{\rm red}$ matched the rate of radical termination ($R_{\rm t}$), which is a characteristic feature for all low ppm ATRP processes.^{36,71}

The mechanism of Na₂S₂O₄-mediated SARA ATRP closely resembles that of Cu⁰-mediated RDRP. 15,39 However, the substitution of Cu⁰ by inorganic sulfites has the advantage of avoiding introduction of additional soluble Cu species into the reaction mixture through supplemental activation and comproportionation reactions. For example, in Cu⁰-mediated SARA ATRP of oligo(ethylene oxide) methyl ether acrylate ($M_n = 480$) in aqueous media, the amount of soluble Cu species gradually increased from initially added 100 ppm to ca. 600 ppm.²¹ In the case of Na₂S₂O₄-mediated SARA ATRP, excellent polymerization control is maintained without increasing the amount of soluble copper in the reaction medium during the reaction (Fig. 7a). As previously mentioned, the decrease of the concentration of soluble copper used in ATRP reactions has been a subject of interest, mainly due to the desire to provide metalfree products for certain applications, e.g., in the biomedical field.72

Effect of the targeted degree of polymerization

The effect of the initial molar ratio of monomer to initiator, the targeted DP, on SARA ATRP was investigated by simulations (Fig. 8). When available, experimental data were superimposed on the results of the simulations, always with very good agreement. In all cases, regardless of the targeted DP, the resulting polymers displayed narrow MWD and good agreement between simulated and theoretical DP. As expected for SARA ATRP the rates of polymerization were proportional to $\sqrt{[RX]_0}$. Finally, lower targeted DPs resulted in smaller fractions of terminated chains $(T_{\rm mol})$. This shows that Na₂S₂O₄-mediated SARA ATRP is suitable for the synthesis of polymers with a wide range of targeted molecular weights. Analogous results were obtained for polymerizations initiated by MBrP (Fig. S13†).

Effect of the amount of CuII deactivator

SARA ATRP mediated by $Na_2S_2O_4$ requires the initial presence of Cu^{II} deactivator complex. This is in contrast to the Cu^{0} -

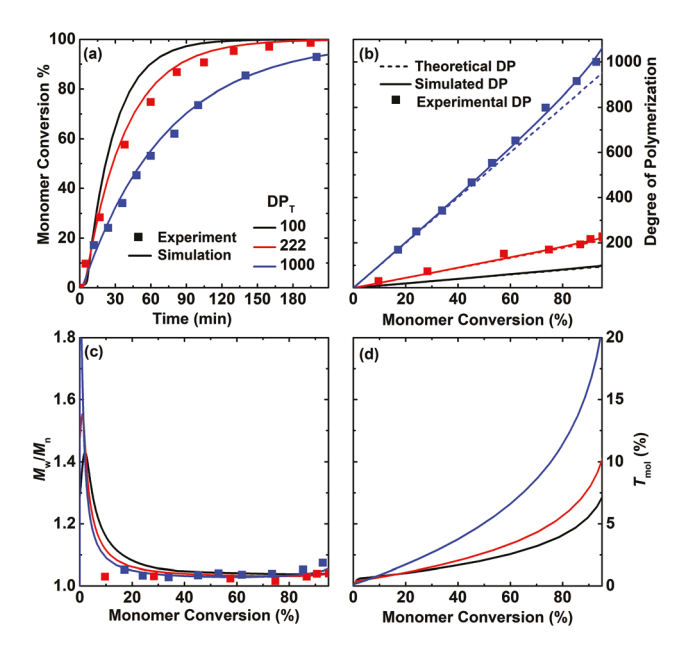


Fig. 8 Simulated (lines) and experimental (squares) kinetic plots for the SARA ATRP of MA in EtOH/H₂O at 30 °C. (a) semilogarithmic kinetic plot, (b) DP vs. monomer conversion, (c) M_n vs. monomer conversion, and (d) $T_{\rm mol}$ vs. monomer conversion. Reaction conditions: MA/EtOH/H₂O = 2/0.9/0.1 (v/v/v); [MA]₀/[EBiB]₀/[Na₂S₂O₄]₀/[Cu^{II}Br₂]₀/[Me₆TREN]₀ = DP/1/1/0.1/0.2, where DP = 100, 222, or 1000, [MA]₀ = 7.4 M.

mediated RDRP, which can be conducted without initially added soluble Cu species, since they can be generated in situ through Cu⁰ activation and comproportionation. When using inorganic sulfites as activators, a lack of initially added Cu^{II} deactivator complex results in an uncontrolled reaction (Fig. S2†). Therefore, simulations with different initial concentrations of Cu^{II} were carried out in order to evaluate the effect of this parameter on the level of control over the polymerization. Again, available experimental data were superimposed to the simulations, confirming the kinetic model. Fig. 9 summarizes the simulations with 4.5, 45, 450, and 1800 ppm of initially added Cu^{II}, expressed as the molar ratio to monomer. The rate of SARA ATRP depends on the rate of radical generation, i.e., supplemental activation and reduction of Cu^{II}. ³⁶ In the case of very low Cu^{II} concentrations, the contribution of the reduction process was negligible, and the rate depended primarily on the rate of supplemental activation, which was constant throughout all simulations. A relatively low concentration of deactivator complex (45 ppm) was required to efficiently control the polymerization and provide good agreement between simulated and theoretical DP as well as low $M_{\rm w}/M_{\rm n}$. Increased amounts of Cu^{II} resulted in a higher concentration of radicals and therefore faster rates of polymerization (Fig. 9a). However, they inevitably resulted in a greater fraction of terminated chains (Fig. 9d), since higher concentration of radicals also leads to a faster rate of termination. The robustness of the model was also confirmed by the good agreement between simulated and experimental data observed even for the low concentration of the deactivation complex (4.5 ppm).

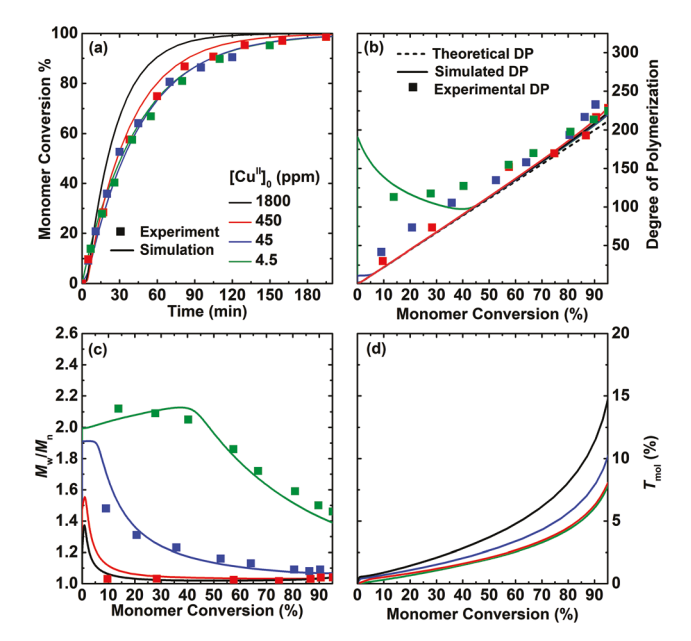


Fig. 9 Simulated (lines) and experimental (squares) kinetic plots for the SARA ATRP of MA in EtOH/H₂O at 30 °C. (a) semilogarithmic kinetic plot, (b) DP vs. monomer conversion, (c) $M_{\rm w}/M_{\rm n}$ vs. monomer conversion, and (d) $T_{\rm mol}$ vs. monomer conversion. Reaction conditions: MA/EtOH/H₂O = 2/0.9/0.1 (v/v/v); [MA]₀/[EBiB]₀/[Na₂S₂O₄]₀/[Cu^{II}Br₂]₀/[Me₆TREN]₀ = 222/1/1/x/2x, where x = 0.001, 0.01, 0.1 or 0.4, [MA]₀ = 7.4 M.

Analogous results were obtained for polymerizations initiated by MBrP (Fig. S14†).

Effect of the amount of SARA agent ([SO₂'-])

The rate of polymerization in a SARA ATRP is proportional to the square root of the amount of SARA agent.³⁶ Indeed, in Cu⁰mediated RDRP the rates were proportional to the $\sqrt{S/V}$, where S is the surface area of Cu^0 and V is the total reaction volume.^{74,75} Correspondingly, in SARA ATRP mediated by inorganic sulfites, polymerization rates should be proportional to the square root of [SO₂*-]; therefore, introduction of higher amounts of the SARA agent should lead to faster polymerizations. However, a higher rate of polymerization is associated with higher concentration of radicals and thus inevitably with higher termination rates. Since propagation is proportional to $[R^*]$ and termination to $[R^*]^2$ this can lead to increased fraction of dead chains and a decrease in chain-end functionality (CEF). Therefore, simulations to evaluate the effect of the amount of the SARA agent on the polymerizations were carried out.

Due to the limited solubility of the inorganic sulfite (Na₂S₂O₄) in the used solvent, the [SO₂·-] could not be modulated simply by altering the amount of Na₂S₂O₄ introduced to the reaction mixture. Instead, experimentally small amounts of water could be added to the system to significantly increase the sulfite solubility and reactivity (and thus increasing [SO₂·-]), without a major influence on other reaction rate coefficients (see next section for more details). For simplicity in modelling, the apparent rate coefficients of activation of

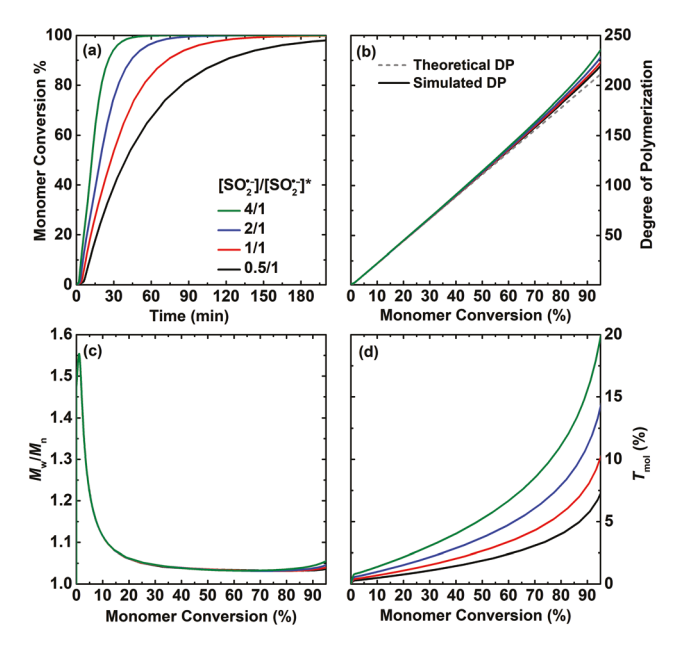


Fig. 10 Simulated kinetic plots for the SARA ATRP of MA in EtOH/H₂O at 30 °C. (a) Semilogarithmic kinetic plot, (b) DP vs. monomer conversion, (c) $M_{\rm w}/M_{\rm n}$ vs. monomer conversion, and (d) $T_{\rm mol}$ vs. monomer conversion. Reaction conditions: MA/EtOH/H₂O = 2/0.9/0.1 (v/v/v); [MA]₀/[EBiB]₀/[Cu^{II}Br₂]₀/[Me₆TREN]₀ = 222/1/0.1/0.2, with [SO₂·-]/[SO₂·-]* = 0.5/1, 1/1, 2/1, and 4/1; [MA]₀ = 7.4 M.

alkyl halides by $SO_2^{\bullet -}$ (k_{a0}^{app} and k_{a0p}^{app} , Scheme 2, reactions (3) and (4)), reduction of Cu^{II}/L by $SO_2^{\bullet -}$ ($k_{red,X-CuL}^{app}$ and $k_{red,X-CuL}^{app}$, Scheme 2, reactions (5) and (6)) were varied appropriately to reflect the change in $[SO_2^{\bullet -}]$, without altering other rate coefficients. Fig. 10 summarizes the simulations with the ratios of $[SO_2^{\bullet -}]/[SO_2^{\bullet -}]^*$ of 4/1, 2/1, 1/1, and 0.5/1 (where $[SO_2^{\bullet -}]^*$ is the concentration of SARA agent under "standard" experimental conditions, *i.e.* $[MA]_0/[EBiB]_0/[Na_2S_2O_4]_0/[Cu^{II}Br_2]_0/[Me_6TREN]_0$ = 222/1/1/0.1/0.2 in $MA/EtOH/H_2O = 2/0.9/0.1$ (v/v/v), at 30 °C, $[MA]_0 = 7.4$ M). As expected, the rates of polymerization scaled with the square root of $[SO_2^{\bullet -}]$. All simulations showed good agreement between simulated and theoretical DP, while MWD remained narrow. Despite minimal differences in DP and M_w/M_n values between simulations, the fraction of terminated chains varied significantly. Retention of CEF at 95% monomer conversion was calculated as 93%, 90%, 85%, and 80%, for

[SO₂·-]/[SO₂·-]* = 0.5/1, 1/1, 2/1, and 4/1, respectively (Fig. 10d). These results indicate that the rate of SARA ATRP can be increased without compromising narrow MWD and targeted DP, but faster reactions do lead to lower CEF. This should be taken into account for the functionalization of chain-ends and for the preparation of block copolymers. Analogous results were obtained for polymerization initiated by MBrP (Fig. S15†).

Effect of water on the polymerization

In a previous paper, we reported how the presence of small amounts of water drastically accelerated the SARA ATRP of MA mediated by sulfites/ $Cu^{II}Br_2/Me_6TREN$ in MA/EtOH mixtures. ²⁶ 5% of water (MA/EtOH/H₂O = 1/0.9/0.1 (v/v/v)) increased k_p^{app} 15 fold with respect to anhydrous MA/EtOH = 1/1 (v/v). Adding 17.5% of water (MA/EtOH/H₂O = 1/0.65/0.35 (v/v/v)) further increased k_p^{app} by a factor of 9. To explain these striking results, the effect of water on the catalytic system composed of a copper complex and sulfites was studied. This is of particular interest as it can provide a better understanding of the large body of work utilizing the so-called "water-accelerated ATRP". ^{76–79} First, the catalyst alone was considered.

The presence of water can affect the activity of the catalyst (i.e. K_{ATRP}) in two ways: (i) by altering Cu^{II}/L redox properties, i.e. the standard reduction potential $(E_{\mathrm{Cu(II)L/Cu(I)L}}^{\circ})$ and (ii) by diminishing the halidophilicity constant of Cu^{II}/L (K_{Br}^{II} , see also Scheme S1†). The properties of the Cu^{II}/Me₆TREN catalyst complex were studied by CV, which was then used to investigate the role of solvents (MA/EtOH/H2O mixtures) on the thermodynamic properties of the catalyst. Table 2 lists the standard reduction potentials of the catalyst in different MA/ EtOH/H₂O mixtures. $E_{\text{Cu(II)L/Cu(I)L}}^{\circ}$ in pure MA is relatively positive, i.e. the catalyst is a weak reducing agent, with low ATRP activity. Adding EtOH to MA (so that MA/EtOH = 2/1 (v/v)) only slightly influences the CV of Cu^{II}/Me₆TREN (Fig. S16†). Thus, EtOH itself did not significantly affect the electrochemical properties of the catalyst. However, Fig. 11a shows that the presence of small amounts of water produced a large cathodic shift of the Cu^{II}/Me₆TREN redox potential. For example, addition of only 3.3% water to MA/EtOH = 2/1 (v/v), so that MA/EtOH/H₂O = 2/0.9/0.1 (v/v/v), shifted $E_{Cu(II)L/Cu(I)L}^{\circ}$ by -155 mV (Table 2, entry 4). Therefore, the presence of water makes the Cu^I/L complex a much more active reducing agent.

Table 2 Electrochemical and thermodynamic parameters of Cu^{II}/Me₆TREN in different solvent mixtures

Entry	MA/EtOH/H ₂ O (v/v/v)	$E_{ m Cu(II)L/Cu(I)L}^{\circ}{}^a$	$E_{\mathrm{CuBr}(\mathrm{II})\mathrm{L/CuBr}(\mathrm{I})\mathrm{L}}^{\circ}\ ^{b}$	$K_{ m Br}^{ m II}/K_{ m Br}^{ m I}$	$I_{\mathrm{p}}^{}d}$
1	1/0/0	0.006	-0.301	1.5×10^{5}	-51
2	2/1/0	0.025	-0.295	2.6×10^{5}	-63
3	2/0.99/0.01	-0.043	-0.293	1.7×10^{4}	-66
4	2/0.90/0.10	-0.130	-0.289	5.0×10^{2}	-78
5	2/0.65/0.35	-0.204	-0.281	2.0×10^{1}	-85
6	0/0/1	-0.439	\sim -0.41^e	$\sim 3 \times 10^{-1}$	N/A^f

^a Calculated as the half-wave potential of Cu^{II}OTf₂/L, Fig. 11a. ^b Calculated as the half-wave potential of Cu^{II}Br₂/L (Fig. S17) or Cu^{II}Br/L⁺. ^c Calculated from eqn (1). ^d The intensity of the catalytic cathodic peak from Fig. 11. ^e Estimated from Fig. S18. ^f The EBiB initiator is not well-soluble in pure water.

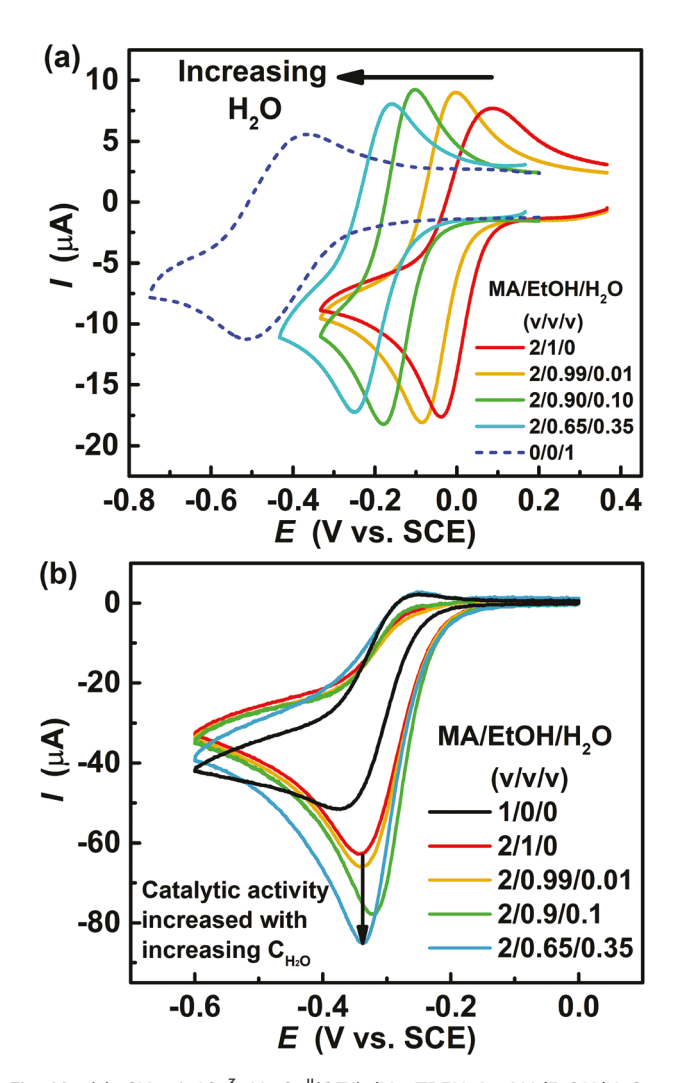


Fig. 11 (a) CV of 10^{-3} M Cu^{II}(OTf)₂/Me₆TREN in MA/EtOH/H₂O at different ratios (a) in the absence and (b) in the presence of 10^{-3} M EBiB. The supporting electrolyte was 0.1 M n-Bu₄NPF₆ in the organic solvent mixtures and Et₄NBF₄ in water. T=30 °C and v=0.1 V s⁻¹.

The activity of an ATRP catalyst also depends on its halidophilicity $(K_{\rm X}^{\rm II})$, 80,81 *i.e.* the catalyst's ability of capturing the halide anion. As discussed above, the presence of water drastically reduces $K_{\rm X}^{\rm II}$ compared to pure organic solvents. A further insight into the decreased ${\rm Cu^{II}}$ halidophilicity is presented in Table 2 where the $K_{\rm Br}^{\rm II}/K_{\rm Br}^{\rm I}$ ratio sharply decreased when small amounts of water were added. The $K_{\rm Br}^{\rm II}/K_{\rm Br}^{\rm I}$ in different MA/EtOH/H₂O mixtures was calculated from eqn (1). $K_{\rm Br}^{\rm II}/K_{\rm Br}^{\rm I}$ predominately depends on $K_{\rm Br}^{\rm II}$, 41,81 therefore its sharp decrease confirmed that the value of $K_{\rm Br}^{\rm II}$ was strongly decreased by adding water.

In conclusion, analysis of the CV curves proved that addition of a small amount of water made the catalyst a better reducing agent (*i.e.* more active), while decreased $\mathrm{Cu^{II}/L}$ halidophilicity resulted in a less active catalyst. The two effects roughly compensated each other, resulting in only a modest increase in catalyst's activity. In fact, experimentally determined k_{a1} increased only two-fold, from $(2.8 \pm 0.6) \times 10^3 \ \mathrm{M^{-1}}$

s⁻¹ to $(6.3 \pm 0.9) \times 10^3 \, \mathrm{M^{-1}} \, \mathrm{s^{-1}}$, when adding 3.3% water to the MA/EtOH = 2/1 (v/v) mixture (see Fig. S19†). The increased activity was validated by CV of Cu^{II}/Me₆TREN in the presence of the EBiB initiator (Fig. 11b), which showed that small amounts of water improved catalytic performance, confirmed by the slightly higher cathodic current, $I_{\rm p}$; see also last column in Table 2.

Conversely, the reactivity of sulfites drastically changed after addition of small amounts of water. The reduction rate of $\mathrm{Cu^{II}Br_2/Me_6TREN}$ by $\mathrm{Na_2S_2O_4}$ was 41 times faster in the presence of only 3.3% of water: $k_{\mathrm{red,X-CuL}}^{\mathrm{app}} = (1.5 \pm 0.01) \times 10^{-6} \mathrm{\ s^{-1}}$ (Fig. S20†) in MeOAc/EtOH = 2/1 (v/v) vs. (6.2 \pm 0.02) \times 10⁻⁵ s⁻¹ (Fig. 2) in MeOAc/EtOH/H₂O = 2/0.9/0.1 (v/v/v). Therefore, it appears that the presence of a polar solvent increased polymerization rate by increasing the solubility of the dithionite or the activity of the SO₂*- SARA agent, resulting in a faster reduction rate of both $\mathrm{Cu^{II}/L}$ and RX.

Nature of the electron transfer (ET) between SO_2 and Cu^{II} or RX

The reduction of Cu^{II} complexes and alkyl halides by SO₂. was investigated to elucidate the ET mechanism of the SO2. radical anion, see Table 3. The reduction rate depended predominately on the standard reduction potential of the substrate (see also Fig. S21†), while it was only slightly influenced by large changes in the molecular structure of the substrates, such as copper complexes with and without bromides, or alkyl halides. This suggests that the reaction followed an outer sphere electron transfer (OSET) process, where there is no particular interaction between the two reacting molecules, SO₂. and Cu^{II}/L or RX. In particular, the presence of -Br in the coordination sphere of Cu^{II} did not favor electron transfer to SO_2 (entry 1 vs. entry 2 in Table 3). In contrast, the presence of -Br drastically increases the ET rate in the atom transfer reaction between CuI/L and RBr or between Br-CuI/L and R. Indeed, it is known that Cu^I complexes reduce alkyl halides via an inner sphere electron transfer (ISET),80 a process that strongly depends on the molecular structure of both catalyst and alkyl halide, because a specific interaction occurs between the two reactants, i.e. formation of a Cu-X-R intermediate.

In conclusion, no evidence of inner sphere interactions was detected in the ET between SO₂. and Cu^{II}Br/Me₆TREN or RBr,

Table 3 Standard reduction potentials and rate coefficients for the ET between the reducing agent SO_2 and different substrates

Entry	Oxidant	E° (V vs. SCE)	$k_{\text{red}} \times [SO_2^{\bullet -}] \text{ or } k_{a0} (s^{-1})$
1 2 3 4 5	Cu^{II}/Me_6TREN^{2+} $Cu^{II}Br/Me_6TREN^{+}$ $Cu^{II}Cl/Me_6TREN^{+}$ $EBiB$ $MBrP$	-0.130 -0.289 -0.345^{a} -0.52^{c} -0.56^{c}	2.3×10^{-4} 6.2×10^{-5} $6.9 \times 10^{-5} b$ 1.2×10^{-5} 9.7×10^{-6}

 $[^]a\mathrm{From}$ Fig. S22. $^b\mathrm{From}$ Fig. S23. $^c\mathrm{In}$ dimethylformamide (DMF) as solvent. 83

which would indicate that they interact by an OSET process. In such processes, reduction of propagating radicals to carbanions is prevented by the low concentration of both reducing agent and R^{\star} , as already observed for other OSET reducing agents.

Conclusions

The determination of the rate coefficients and the validation of the proposed kinetic model for the $Na_2S_2O_4/Cu^{II}Br_2/Me_6TREN$ -catalyzed RDRP of MA in EtOH/H₂O mixtures confirmed that the reaction mechanism followed a typical SARA ATRP process. It was shown that the SO_2 radical anion, resulting from the dissolution of $Na_2S_2O_4$ and subsequent dissociation of the dithionite anion, can activate alkyl halides, in a supplemental activation reaction. It can also reduce the $Cu^{II}Br_2/Me_6TREN$ deactivator complex.

The presence of a small amount of water drastically increased the rate of polymerization but only marginally increased the activity of the copper catalyst, indicating that water strongly influenced the solubility and/or activity of the dithionite SARA agent without significantly affecting other polymerization parameters. The developed kinetic model is a valuable tool, which can be used to further explore and improve the reported SARA ATRP system.

Conflicts of interest

The authors declare no competing financial interest.

Acknowledgements

Financial support from NSF (CHE 1707490) and NIH (R01DE020843) is gratefully acknowledged. P. K. acknowledges Dr Konrad M. Weis Fellowship in Chemistry. P. M. acknowledges FCT-MCTES for her Post-Doctoral Fellowship (Project PTDC/CTMPOL/6138/2014). C. M. R. A. acknowledges FCT-MCTES for his Ph.D. scholarship (SFRH/BD/88528/ 2012). J. F. J. C. acknowledges FCT-MCTES for financial support (PTDC/CTMPOL/6138/2014 & CMUP-ERI/TIC/0021/ 2014) and the Carnegie Mellon Portugal Faculty Exchange Program for supporting his Visiting Scholar program at CMU in 2016. Part of project was also supported by Project Flexivinil (QREN 3320). The 1H NMR data was collected at the UC-NMR facility which is supported in part by FEDER - European Regional Development Fund through the COMPETE Programme (Operational Programme for Competitiveness) and by National Funds through FCT - Fundação para a Ciência e a Tecnologia (Portuguese Foundation for Science Technology) through grants REEQ/481/QUI/2006, RECI/ QEQ-QFI/0168/2012, CENTRO-07-CT62-FEDER-002012, and Rede Nacional de Ressonância Magnética Nuclear (RNRMN).

Notes and references

- 1 K. Matyjaszewski and W. A. Braunecker, in *Macromol. Mater. Eng*, Wiley-VCH Verlag GmbH & Co. KGaA, 2007, pp. 161–215.
- 2 K. Matyjaszewski and N. V. Tsarevsky, J. Am. Chem. Soc., 2014, 136, 6513–6533.
- 3 J.-S. Wang and K. Matyjaszewski, *J. Am. Chem. Soc.*, 1995, 117, 5614–5615.
- 4 N. Ayres, Polym. Rev., 2011, 51, 138-162.
- 5 K. Matyjaszewski, *Macromolecules*, 2012, **45**, 4015–4039.
- 6 K. Matyjaszewski and J. Xia, Chem. Rev., 2001, 101, 2921– 2990.
- 7 W. Jakubowski and K. Matyjaszewski, *Angew. Chem., Int. Ed.*, 2006, **118**, 4594–4598.
- 8 K. Matyjaszewski, W. Jakubowski, K. Min, W. Tang, J. Huang, W. A. Braunecker and N. V. Tsarevsky, *Proc. Natl. Acad. Sci. U. S. A.*, 2006, **103**, 15309–15314.
- 9 A. J. D. Magenau, N. C. Strandwitz, A. Gennaro and K. Matyjaszewski, *Science*, 2011, 332, 81–84.
- 10 X. Pan, M. A. Tasdelen, J. Laun, T. Junkers, Y. Yagci and K. Matyjaszewski, *Prog. Polym. Sci.*, 2016, **62**, 73–125.
- 11 P. V. Mendonça, A. C. Serra, J. F. J. Coelho, A. V. Popov and T. Guliashvili, *Eur. Polym. Chem.*, 2011, 47, 1460–1466.
- 12 Y. Zhang, Y. Wang and K. Matyjaszewski, *Macromolecules*, 2011, 44, 683–685.
- 13 C. M. R. Abreu, P. V. Mendonça, A. C. Serra, J. F. J. Coelho, A. V. Popov and T. Guliashvili, *Macromol. Chem. Phys.*, 2012, 213, 1677–1687.
- 14 C. M. R. Abreu, P. V. Mendonça, A. C. Serra, A. V. Popov, K. Matyjaszewski, T. Guliashvili and J. F. J. Coelho, ACS Macro Lett., 2012, 1, 1308–1311.
- 15 D. Konkolewicz, Y. Wang, M. Zhong, P. Krys, A. A. Isse, A. Gennaro and K. Matyjaszewski, *Macromolecules*, 2013, 46, 8749–8772.
- 16 J. P. Mendes, F. Branco, C. M. R. Abreu, P. V. Mendonça, A. C. Serra, A. V. Popov, T. Guliashvili and J. F. J. Coelho, ACS Macro Lett., 2014, 3, 858–861.
- 17 N. J. Treat, H. Sprafke, J. W. Kramer, P. G. Clark, B. E. Barton, J. Read de Alaniz, B. P. Fors and C. J. Hawker, J. Am. Chem. Soc., 2014, 136, 16096–16101.
- 18 X. Pan, M. Lamson, J. Yan and K. Matyjaszewski, *ACS Macro Lett.*, 2015, 4, 192–196.
- 19 X. Liu, L. Zhang, Z. Cheng and X. Zhu, *Polym. Chem.*, 2016, 7, 689–700.
- 20 V. Percec, T. Guliashvili, J. S. Ladislaw, A. Wistrand, A. Stjerndahl, M. J. Sienkowska, M. J. Monteiro and S. Sahoo, J. Am. Chem. Soc., 2006, 128, 14156–14165.
- 21 D. Konkolewicz, P. Krys, J. R. Góis, P. V. Mendonça, M. Zhong, Y. Wang, A. Gennaro, A. A. Isse, M. Fantin and K. Matyjaszewski, *Macromolecules*, 2014, 47, 560–570.
- 22 T. Guliashvili, P. V. Mendonça, A. C. Serra, A. V. Popov and J. F. J. Coelho, *Chem. Eur. J.*, 2012, **18**, 4607–4612.
- 23 Y. Wang, M. Zhong, W. Zhu, C.-H. Peng, Y. Zhang, D. Konkolewicz, N. Bortolamei, A. A. Isse, A. Gennaro and K. Matyjaszewski, *Macromolecules*, 2013, 46, 3793–3802.

- 24 D. Konkolewicz, Y. Wang, P. Krys, M. Zhong, A. A. Isse, A. Gennaro and K. Matyjaszewski, *Polym. Chem.*, 2014, 5, 4396–4417.
- 25 Food Additive Status List, *U.S. Food and Drug Administration, U.S. Department of Health and Human Services*, Silver Spring, Maryland, USA, https://www.fda.gov/food/ingredientspackaginglabeling/foodadditivesingredients/ucm091048.htm, Accessed September 13th, 2017.
- 26 C. M. R. Abreu, A. C. Serra, A. V. Popov, K. Matyjaszewski, T. Guliashvili and J. F. J. Coelho, *Polym. Chem.*, 2013, 4, 5629–5636.
- 27 J. R. Gois, D. Konkolewic, A. V. Popov, T. Guliashvili, K. Matyjaszewski, A. C. Serra and J. F. J. Coelho, *Polym. Chem.*, 2014, 5, 4617–4626.
- 28 J. R. Gois, N. Rocha, A. V. Popov, T. Guliashvili, K. Matyjaszewski, A. C. Serra and J. F. J. Coelho, *Polym. Chem.*, 2014, 5, 3919–3928.
- 29 J. P. Mendes, F. Branco, C. M. R. Abreu, P. V. Mendonça, A. V. Popov, T. Guliashvili, A. C. Serra and J. F. J. Coelho, *ACS Macro Lett.*, 2014, 3, 544–547.
- 30 J. R. C. Costa, P. V. Mendonça, P. Maximiano, A. C. Serra, T. Guliashvili and J. F. J. Coelho, *Macromolecules*, 2015, 48, 6810–6815.
- 31 P. Maximiano, J. P. Mendes, P. V. Mendonça, C. M. R. Abreu, T. Guliashvili, A. C. Serra and J. F. J. Coelho, *J. Polym. Sci., Part A: Polym. Chem.*, 2015, **53**, 2722–2729.
- 32 J. P. Mendes, P. V. Mendonca, P. Maximiano, C. M. R. Abreu, T. Guliashvili, A. C. Serra and J. F. J. Coelho, *RSC Adv.*, 2016, **6**, 9598–9603.
- 33 C. M. R. Abreu, L. Fu, S. Carmali, A. C. Serra, K. Matyjaszewski and J. F. J. Coelho, *Polym. Chem.*, 2017, 8, 375–387.
- 34 M. Wulkow, Macromol. React. Eng., 2008, 2, 461-494.
- 35 H. Schroeder, J. Buback, J. Schrooten, M. Buback and K. Matyjaszewski, *Macromol. Theory Simul.*, 2014, 23, 279–287.
- 36 P. Krys, T. G. Ribelli, K. Matyjaszewski and A. Gennaro, *Macromolecules*, 2016, **49**, 2467–2476.
- 37 M. Ciampolini and N. Nardi, *Inorg. Chem.*, 1966, 5, 41-44.
- 38 C.-H. Peng, M. Zhong, Y. Wang, Y. Kwak, Y. Zhang, W. Zhu, M. Tonge, J. Buback, S. Park, P. Krys, D. Konkolewicz, A. Gennaro and K. Matyjaszewski, *Macromolecules*, 2013, 46, 3803–3815.
- 39 M. Zhong, Y. Wang, P. Krys, D. Konkolewicz and K. Matyjaszewski, *Macromolecules*, 2013, **46**, 3816–3827.
- 40 S. M. Lough and J. W. McDonald, *Inorg. Chem.*, 1987, 26, 2024–2027.
- 41 N. Bortolamei, A. A. Isse, V. B. Di Marco, A. Gennaro and K. Matyjaszewski, *Macromolecules*, 2010, 43, 9257–9267.
- 42 M. Fantin, A. A. Isse, A. Gennaro and K. Matyjaszewski, *Macromolecules*, 2015, **48**, 6862–6875.
- 43 F. Lorandi, M. Fantin, A. A. Isse and A. Gennaro, *Polymer*, 2015, 72, 238–245.
- 44 C. P. Andrieux, J. M. Dumas-Bouchiat and J. M. Saveant, J. Electroanal. Chem. Interfacial Electrochem., 1978, 87, 55– 65

45 C. P. Andrieux, J. M. Dumas-Bouchiat and J. M. Saveant, J. Electroanal. Chem. Interfacial Electrochem., 1978, 87, 39–53.

- 46 C. P. Andrieux, C. Blocman, J. M. Dumas-Bouchiat, F. M'Halla and J. M. Savéant, J. Electroanal. Chem. Interfacial Electrochem., 1980, 113, 19–40.
- 47 C. P. Andrieux, I. Gallardo, J. M. Savaent and K. B. Su, *I. Am. Chem. Soc.*, 1986, **108**, 638–647.
- 48 D. Lexa, J. M. Saveant, K. B. Su and D. L. Wang, *J. Am. Chem. Soc.*, 1987, **109**, 6464–6470.
- 49 A. Cardinale, A. A. Isse and A. Gennaro, *Electrochem. Commun.*, 2002, 4, 767–772.
- 50 A. A. Isse and A. Gennaro, *J. Phys. Chem. A*, 2004, **108**, 4180–4186.
- 51 C. Costentin, M. Robert and J.-M. Savéant, *J. Am. Chem. Soc.*, 2005, **127**, 12154–12155.
- 52 A. J. Bard and L. R. Faulkner, in *Electrochemical Methods: Principles and Applications*, John Wiley & Sons, New York, 2001, ch. 12.
- 53 V. A. Benderskii, A. G. Krivenko and A. A. Ovchinnikov, J. Electroanal. Chem. Interfacial Electrochem., 1980, 111, 19– 40
- 54 M. Fantin, A. A. Isse, K. Matyjaszewski and A. Gennaro, *Macromolecules*, 2017, **50**, 2696–2705.
- 55 M. Fantin, A. A. Isse, N. Bortolamei, K. Matyjaszewski and A. Gennaro, *Electrochim. Acta*, 2016, **222**, 393–401.
- 56 C. Y. Lin, M. L. Coote, A. Petit, P. Richard, R. Poli and K. Matyjaszewski, *Macromolecules*, 2007, 40, 5985– 5994.
- 57 R. M. Shirke, A. Chaudhari, N. M. More and P. B. Patil, J. Chem. Eng. Data, 2000, 45, 917–919.
- 58 R. R. Nazmutdinov, G. A. Tsirlina, Y. I. Kharkats, O. A. Petrii and M. Probst, *J. Phys. Chem. B*, 1998, **102**, 677–686.
- 59 W. A. Braunecker, T. Pintauer, N. V. Tsarevsky, G. Kickelbick and M. Krzysztof, J. Organomet. Chem., 2005, 690, 916–924.
- 60 W. Tang, N. V. Tsarevsky and K. Matyjaszewski, *J. Am. Chem. Soc.*, 2006, **128**, 1598–1604.
- 61 Y. Wang, Y. Kwak, J. Buback, M. Buback and K. Matyjaszewski, ACS Macro Lett., 2012, 1, 1367–1370.
- 62 W. Tang, Y. Kwak, W. Braunecker, N. V. Tsarevsky, M. L. Coote and K. Matyjaszewski, *J. Am. Chem. Soc.*, 2008, 130, 10702–10713.
- 63 H. Fischer and L. Radom, Angew. Chem., Int. Ed., 2001, 40, 1340–1371.
- 64 B. Knuhl, S. Marque and H. Fischer, *Helv. Chim. Acta*, 2001, **84**, 2290–2300.
- 65 M. Buback, A. Kuelpmann and C. Kurz, *Macromol. Chem. Phys.*, 2002, **203**, 1065–1070.
- 66 W. A. Braunecker, N. V. Tsarevsky, A. Gennaro and K. Matyjaszewski, *Macromolecules*, 2009, 42, 6348–6360.
- 67 C. Barner-Kowollik, S. Beuermann, M. Buback, P. Castignolles, B. Charleux, M. L. Coote, R. A. Hutchinson, T. Junkers, I. Lacik, G. T. Russell, M. Stach and A. M. van Herk, *Polym. Chem.*, 2014, 5, 204–212.

68 S. Beuermann, *Macromol. Rapid Commun.*, 2009, **30**, 1066–1088.

- 69 M. Buback, M. Egorov, R. G. Gilbert, V. Kaminsky, O. F. Olaj, G. T. Russell, P. Vana and G. Zifferer, *Macromol. Chem. Phys.*, 2002, **203**, 2570–2582.
- 70 S. G. Mayhew, Eur. J. Biochem., 1978, 85, 535-547.
- 71 P. Krys and K. Matyjaszewski, *Eur. Polym. Chem.*, 2017, **89**, 482–523.
- 72 K. S. Egorova and V. P. Ananikov, *Angew. Chem., Int. Ed.*, 2016, 55, 12150–12162.
- 73 M. Zhong and K. Matyjaszewski, *Macromolecules*, 2011, 44, 2668–2677.
- 74 N. H. Nguyen, B. M. Rosen, G. Lligadas and V. Percec, *Macromolecules*, 2009, 42, 2379–2386.
- 75 Y. Zhang, Y. Wang, C.-H. Peng, M. Zhong, W. Zhu, D. Konkolewicz and K. Matyjaszewski, *Macromolecules*, 2012, 45, 78–86.

- 76 W. Huang, J.-B. Kim, M. L. Bruening and G. L. Baker, *Macromolecules*, 2002, 35, 1175–1179.
- 77 J. Ye and R. Narain, J. Phys. Chem. B, 2009, 113, 676-681.
- 78 G. Panzarasa, G. Soliveri and V. Pifferi, *J. Mater. Chem. C*, 2016, 4, 340–347.
- 79 K. L. Robinson, M. A. Khan, M. V. de Paz Báñez, X. S. Wang and S. P. Armes, *Macromolecules*, 2001, 34, 3155–3158.
- 80 C. Y. Lin, M. L. Coote, A. Gennaro and K. Matyjaszewski, J. Am. Chem. Soc., 2008, 130, 12762–12774.
- 81 S. Lanzalaco, M. Fantin, O. Scialdone, A. Galia, A. A. Isse, A. Gennaro and K. Matyjaszewski, *Macromolecules*, 2017, 50, 192–202.
- 82 X. Pan, C. Fang, M. Fantin, N. Malhotra, W. Y. So, L. A. Peteanu, A. A. Isse, A. Gennaro, P. Liu and K. Matyjaszewski, *J. Am. Chem. Soc.*, 2016, **138**, 2411–2425.
- 83 A. A. Isse, C. Y. Lin, M. L. Coote and A. Gennaro, *J. Phys. Chem. B*, 2011, **115**, 678–684.